Femtosecond Optical Spectroscopy and Scanning Probe Microscopy

M. J. Feldstein, P. Vöhringer,† W. Wang, and N. F. Scherer*,‡

Laboratory for the Research on the Structure of Matter, The University of Pennsylvania, Philadelphia, Pennsylvania 19104

Received: June 28, 1995; In Final Form: December 7, 1995[⊗]

A new technique and an apparatus which provide a promising approach for simultaneous spatial and temporal resolution of optically initiated dynamics at interfaces are presented. The method, based on the integration of femtosecond optical spectroscopy and scanning probe microscopy (FOS-SPM), is shown to be capable of spatially localizing optical measurements at an interface via coupling of the optical field to a metal SPM tip. FOS-SPM measurements are shown to obtain femtosecond time resolution in optically induced processes via an optical pump−probe correlation method. The ability of FOS-SPM to identify and differentiate between different optoelectronic mechanisms is demonstrated. The potentially broad applicability of the technique for the study of interfacial and adsorbate dynamics of numerous systems with simultaneous high spatial and temporal resolution is discussed.

I. Introduction

Chemical dynamics occurring at interfaces[1,2] are central to applied problems in the fields of electrochemistry, semiconductor processing, and nanoscale device technology. The experimental measurement of the rate of reaction at individual surface sites and surface features is essential for an improved understanding of chemical processes at interfaces. An important advance in the realm of interfacial studies would therefore be the development of a capability to study surface dynamics one surface region at a time rather than measuring the averaged response of an ensemble of surface sites.

Scanning probe microscopy (SPM) has developed over the last 13 years from a single technique to include a large series of techniques capable of imaging with resolution in the suboptical wavelength to atomic scale range.[3] The common feature of SPM techniques is that they operate by detecting and exploiting localized probe−surface interactions while scanning the probe tip in space. The original SPM technique is scanning tunneling microscopy (STM), which is capable of imaging the surface electronic state "topography" of electrically conductive materials with atomic resolution.[4] This is achieved by measuring the electron tunneling current between the sharp probe tip and the surface, thereby achieving atomic scale position resolution.

Time-resolved laser spectroscopy is the only technique capable of directly examining chemical reactions on the time scale of the fastest chemical process.[5,6] Currently, the state of art in laser technology enables time resolution on the order of several femtoseconds.[7] The combination of pulsed laser and SPM technologies would enable the simultaneous temporally and spatially resolved capability useful for unique examination of interfacial processes. Ideally, this marriage would yield the best of both techniques and result in femtosecond time-resolved scanning probe microscopy (FTR-SPM).

Experiments have previously demonstrated the viability of coupling optical spectroscopy and STM to yield new optical scanning probe microscopy techniques. For example, a number of excellent experiments have been performed with optically enhanced or mediated STM. Specht *et al*. have used an STM tip as a local probe of resonantly excited surface plasmons to generate a near-field optical image with 3 nm resolution.[8] Surface plasmon excitations have also been exploited by Rücker *et al*. to yield enhanced contrast in an STM image.[9] A new mode of STM operation, capable of atomic resolution, where optical frequency mixing in the tunneling gap is monitored as feedback for tip−sample distance control has been demonstrated in experiments performed by Völcker *et al*.[10] Recently, Bachelot *et al*. have demonstrated ∼100 nm resolution based on the localized interaction of a vibrating SPM tip with an optical field at a surface.[11] Other experiments have used combined STM-optical processes for such applications as nanoprocessing[12] and photoassisted STM spectroscopy of semiconductors.[13−15]

A limited number of experiments on time-resolved scanning probe microscopy have been published.[16−19] While each of these projects offers unique and revolutionary advances in the field, the scope of these projects has typically been narrowly focused and/or limited in temporal capability. Hamers and Cahill[16] pioneered the idea of an optical pump−probe correlation technique for time-resolved STM, detecting nanosecond to microsecond responses in semiconductors. Freeman and Nunes have demonstrated picosecond resolution in STM using two photoconductive switches to inject voltage pulses into their sample, a gold transmission line.[17] Weiss *et al*. have also achieved picosecond resolution using a similar sample but with the addition of a photoconductive switch to gate the tunneling current.[18] These latter approaches, although elegant and promising with respect to continued development, are limited by the relaxation time of their photoconductive switches as well as by complex capacitance and charging effects. Gerber *et al*.[19] have also presented some preliminary work on time-resolved STM via pump−probe correlation. However, a generalized FTR-SPM scheme, capable of studying a wide range of systems, has not yet been clearly demonstrated.

This paper reports on one promising approach to FTR-SPM. The preliminary development and first application of an apparatus and techniques to couple femtosecond optical spectroscopy with scanning probe microscopy (FOS-SPM) are presented. This approach to time-resolved scanning probe microscopy takes advantage of spatially localized interactions of the SPM tip with an illuminated or optically excited surface

† Deutsche Forschungsgemeinschaft Postdoctoral Fellow. Present address: Max Planck Institute für Biophysikalische Chemie, Göttingen, Germany.

‡ David and Lucille Packard Foundation Fellow.

[⊗] Abstract published in *Advance ACS Abstracts,* February 15, 1996.

0022-3654/96/20100-4739$12.00/0

or, ultimately, adsorbate. The coupling of SPM and femtosecond spectroscopy techniques is achieved through several different modes of interaction between the two. First, operating in the normal tunneling current mode as a scanning tunneling microscope to directly probe the surface electronic local density of states (LDOS),[20] optically induced perturbations of the electron LDOS can be detected and spatially resolved. Additionally, operating as a scanning, spatially localized electrode, other electronic changes can be probed using an STM apparatus. For example, an appropriately designed tip can be used as a localized detector for spatially resolved photoemission studies. These electronic processes can be time-resolved via ultrafast pump−probe correlation spectroscopy to provide temporal resolution in the measurement. Second, the close proximity of the probe tip (0.1−10 nm) to a surface can be used to cause a localized perturbation of the electronic environment of the system by changing the dielectric constant at the interface or acting as a scattering center for optical excitation.[8,11] The metal tip can also electronically couple to optically excited chromophores and perturb the excited state's lifetime.[21] The resulting spatially localized tip-induced perturbation can then be probed in the time domain via pump−probe techniques which are sensitive to the (electronic) state of the system while being scanned across the surface. The femtosecond optical spectroscopy and scanning probe microscopy (FOS-SPM) apparatus reported here, although designed to achieve correlated spatial and temporal resolution, has not yet attained the full potential of FTR-SPM. However, it is envisioned that this technique could be applied to the time-resolved, spatially localized study and detection of optical excitation of adsorbate−surface charge transfer states or perturbations in surface−adsorbate coupling due to optically induced changes in adsorbate electronic structure.

In the present paper, the temporal and spatial dynamics of optically induced excitation of the surface plasmon polariton (SPP) modes of a metal film, prepared using the Kretschmann−Raether attenuated total reflection (ATR) geometry,[22,23] have been probed in a number of ways. First, SPM tip-modulated optical measurements have been taken. These measurements are a step toward localization, beyond the diffraction limit, of femtosecond spectroscopic probes of surface dynamics. Among the experiments described herein are SPM tip-modulated surface second harmonic generation and ATR studies, both measured as a function of pump−probe temporal separation.

Second, two different mechanisms of photoinduced signal generation have been identified through the use of the biased SPM tip as a localized current or voltage probe. These two mechanisms, surface plasmon polariton assisted multiphoton ionization (SPP-MPI) and evanescent field rectification (EFR), are uniquely described through their contrasting responses in pump−probe temporal separation (i.e., time delay) as well as tunneling junction bias, optical incidence angle, laser power, and gap distance. While aspects of each of these two mechanisms have been studied previously, we believe that the spatially localized femtosecond time scale measurements reported here, and their associated dependence on a number of parameters, are unique and constitute an important result with broad potential application.

In section II, the experimental apparatus and the signal detection techniques for FOS-SPM are outlined. The preliminary results of FOS-SPM as applied to the study of a thin Ag film are presented in section III. These results, and an explanation of the optoelectronic mechanisms involved, are discussed in section IV. Finally, the present approach is compared to other spatially localized optical measurements and future applications of FOS-SPM are suggested in section V.

II. Experimental Section

Several important practical experimental considerations have been addressed during the process of developing and implementing this research. Of primary importance, the system to be studied must be simultaneously accessible to both probes, SPM and optical pulses, with minimal direct interaction between the two. For example, the probe tip should not shadow or block the excitation of the interface and should not be heated by the light pulses. With these considerations in mind, the experimental setup, shown in Figure 1, has been designed on the basis of the Kretschmann−Raether ATR geometry. This configuration allows for the simultaneous probing of the surface from above by the SPM and for optical excitation and detection from below via the ATR signal as well as the surface-sensitive second-harmonic signal generated at the interface. Additionally, optical excitation in this geometry is inherently sensitive to electronic dynamics at the interface due to its strong dependence on the complex dielectric constants of each layer in the interface system.

As illustrated in Figure 1A, the optical source is an argon ion laser (Laser Ionics) pumped, home-built, *x*-fold Ti:sapphire laser[24] that routinely generates 40 fs pulses centered at 760 nm at a 90 MHz repetition rate. The pump−probe optical arrangement is of typical design, with a prism delay line to compensate for dispersion of the pulse, a 50% beam splitter to separate pump and probe pulse trains, a fixed delay line, and a stepped delay line (Newport Micro Control, 0.1 μm resolution). The surface reflections of both pump and probe beams from an uncoated substrate are focused into a BBO doubling crystal prior to the interface arrangement. The resultant second-harmonic signal generated in this doubling crystal is used to determine the pulse duration from the pump−probe cross-correlation.

The ATR experimental configuration shown in Figure 1B is designed for performing both optical and tunneling current measurements with the capacity for simultaneous detection of multiple signals in a number of configurations. The pump and probe pulse trains are focused through a 20 cm lens onto the hypotenuse of a right angle fused silica prism at approximately 45° relative to the surface normal and can be walked in one dimension (*X* axis) across the surface parallel to the beam propagation direction. The prism is mounted onto a goniometer (Melles Griot), to allow for fine adjustment of the incident angle, and a translation stage, to allow positioning of the surface in the *Y* axis, *i.e.*, perpendicular to the incoming beams. A modified STM probe (Digital Instruments) is mounted above the prism with coarse positioning adjustments for the *X*, *Y*, and *Z* axes in addition to the piezo tube fine 3-D positioning.

Three separate pump−probe−SPM configurations are implemented. First, optical signals are recorded in the forward direction after reflection from the interface on the prism hypotenuse. Both the reflected fundamental light and the surface-generated second-harmonic light can be detected individually through a combination of apertures and optical filters and/or a monochromator. For measurements without spatial selectivity, the optical signals are detected with a photomultiplier tube (Hamamatsu), amplified and processed though a lock-in amplifier (SRS850) referenced to an optical chopper in the pump (and/or probe) beam, and recorded as a function of pump−probe temporal separation.

Second, for spatially localized spectroscopic measurements, the optical signals are detected, processed, and recorded as before except that the lock-in amplifier is referenced to high-frequency (∼2 kHz) small-amplitude (1−10 nm) modulation of the SPM tip−surface separation; an optical chopper is not used.

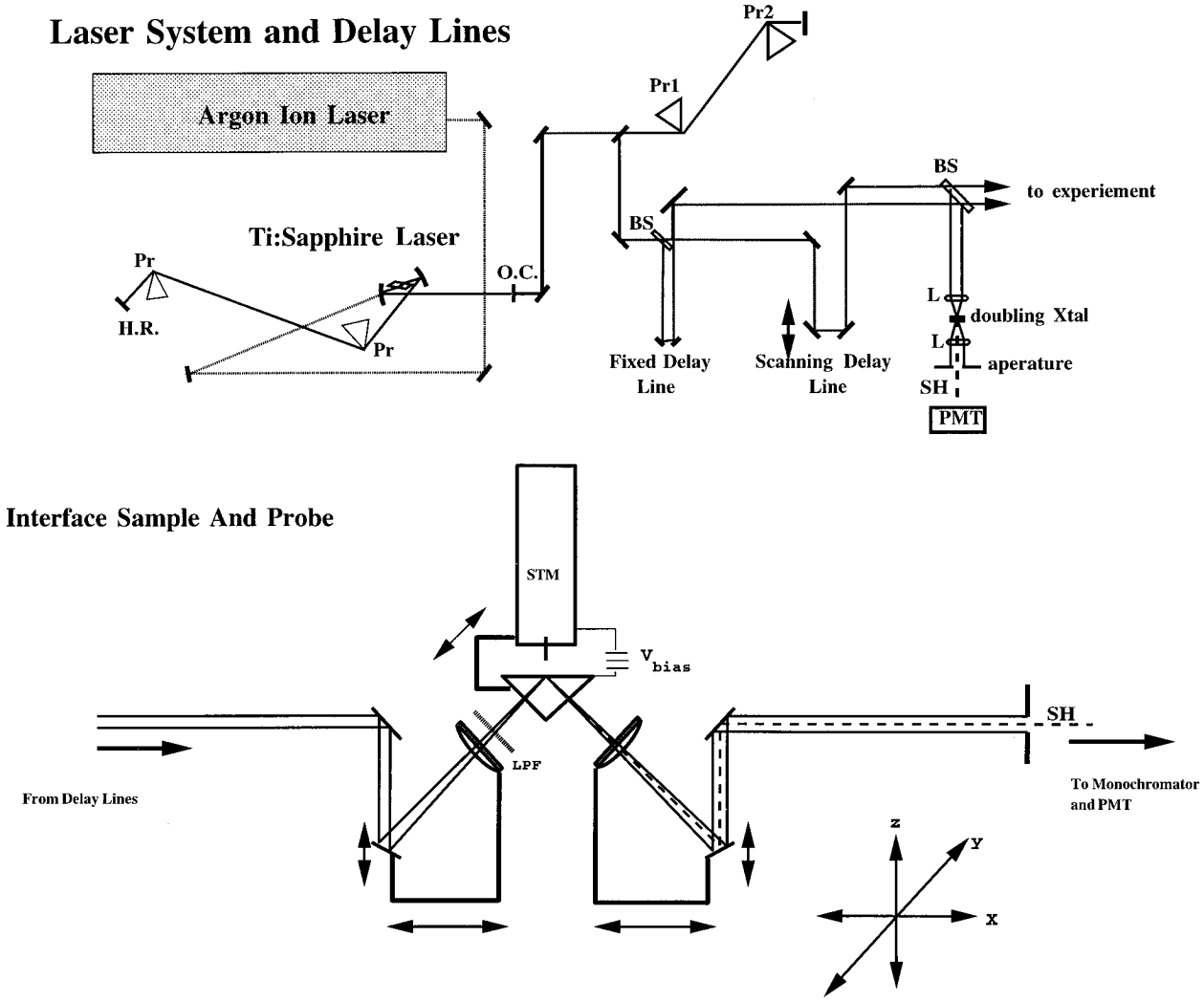

Figure 1. Experimental schematic of laser system (A, top) and interface sample and probe geometry (B, bottom). The laser system illustrated is an argon ion laser pumped home-built Ti:sapphire laser with intracavity prisms, Pr; high reflector end mirror, H.R.; and 6% output coupler. The extracavity optical arrangement consists of prisms for dispersion compensation, Pr1, Pr2; a 50% beam splitter to generate pump and probe beams, BS; fixed and variable delay lines; and a window to obtain surface reflections for cross-correlation measurements, B.S. The interface sample and probe apparatus shown consists of a pair of 20 cm focal length lenses; a long pass filter, LPF; a fused silica prism mounted on a goniometer; an SPM scanner, STM; and an aperture.

Third, photoinduced signals are detected with the modified SPM using a mechanically cut Pt:Ir (80:20) tip and its internal preamplifier and are processed through the lock-in amplifier referenced to an optical chopper in the probe beam. The preamplifier is a two-stage device. The first stage consists of a current-to-voltage converter, with a gain of 10^6 V/A, and the second stage is a voltage amplifier, with a gain of 10^2. Thus, the preamplifier yields a net gain of 10^8 V/A for detected currents and a 10^2 gain for detected voltages. One consequence of this design is that although both current and voltage are amplified, it is not possible to distinguish between the detection of a voltage and a current on the basis of the preamplifier's response alone. An understanding of the optoelectronic process being studied is necessary for this to be determined. Signals are recorded as a function of temporal delay between pump and probe pulses as well as other parameters such as optical incidence angle, junction bias, laser power, and tip−surface separation. For simultaneous electronic and optical measurements, the SPM signal was processed through the digital lock-in and the optical signal through an analog lock-in amplifier (SRS510) referenced to the same phase and frequency.

III. Results

The experimental apparatus and techniques of FOS-SPM have been applied to the study of thin Ag films. First, surface-sensitive optical spectroscopy has been performed in the Kretschmann Raether-ATR geometry on these thin Ag films.[22] Localization of these measurements has been carried out by coupling the optical response to SPM tip motions. In these measurements, the metallic SPM tip is used to induce a localized perturbation and act as a scattering center for the optically generated, plane wave surface plasmon polaritons. Second, two distinct mechanisms producing a photoinduced signal detected via the SPM probe, SPP-MPI and EFR, are characterized in the following data. The two processes are distinguished primarily by tuning or detuning the film/prism angular orientation from the ATR resonance condition. In these data, the biased SPM tip operates as a spatially localized electrode to detect photoinduced current in the case of SPP-MPI and voltage in the case of EFR. Typically, the "steady state" STM response (*i.e.*, the non-photo-induced tunneling current) is monitored for tip positioning but does not contribte to the lock-in amplifier processed data.

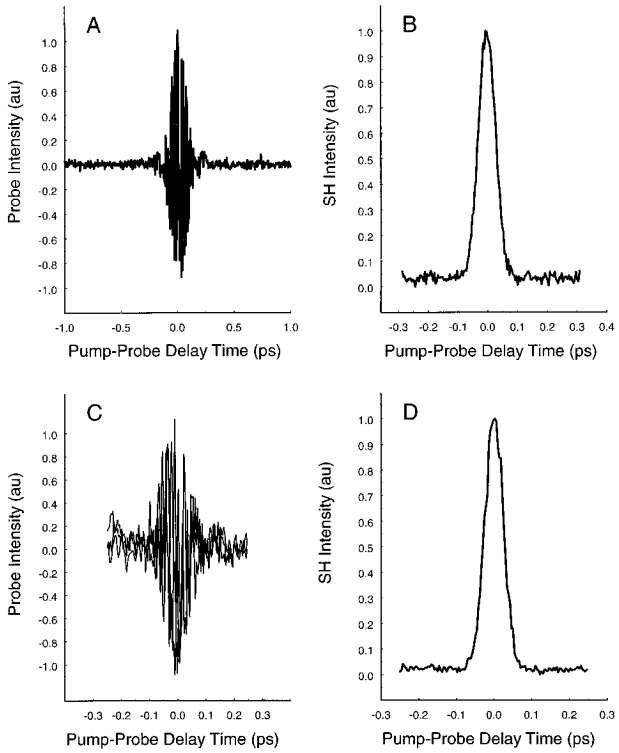

Figure 2. (A) Time dependent pump−probe signal from Ag film. (B) Normalized time dependent surface-generated second-harmonic signal from Ag film. (C) Spatially localized time dependent pump−probe signal from Ag film, recorded as a function of localized 2 KHz STM tip modulation. Three scans are shown to illustrate the interferometric pattern. (D) Spatially localized time dependent surface-generated second-harmonic signal from Ag film, recorded as a function of 2 kHz STM tip modulation; normalized.

A. Surface Sensitive Optical Spectroscopy. Surface sensitive optical spectroscopy was performed in the ATR geometry on thin (525 Å) Ag films[25] vacuum deposited on the prism hypotenuse. The detected signals were the optical responses measured with a PMT located after the sample. Specifically, pump−probe correlation and SHG measurements were both performed to probe the excitation dynamics at the interface. The surface area examined was determined by the approximately 50 μm radius spot size of the focused pump and probe beams overlapped on the surface. These measurements were extremely sensitive to the incident angle (<0.1°) and also showed two additional interesting features. First, when the pump and probe pulses were overlapped both spatially and temporally on the surface, a stable interference pattern was observed (with a 25× telescope) with fringes aligned parallel to the direction of beam propagation. The spacing of the fringes was a function of the crossing angle of the two beams. A second characteristic of these measurements was that the forward reflected beams showed, under the proper conditions, a dark horizontal band through the middle 5−10% of their profile. The contrast ratio of this dark band was approximately 10:1, on the basis of its minimum as compared to the beam's maximum intensity.

Figure 2A shows the pump−probe response from the thin Ag film. The pump−probe measurement exhibits the characteristic pattern of an electric field interference (*i.e.*, vertical symmetry with respect to the baseline) around the zero-of-time. The amplitude of the interference is maximal at the ATR angle (*i.e.*, at the SPP-resonance condition), but a smaller interference contribution is also observed away from the ATR resonance angle. The interference contribution to both signals is averaged to zero either through repetitive scan signal averaging or through continuous, small amplitude (λ/2) modulations of the probe's path length to vary the phase relationship between the pump and probe beams. Path length modulations were introduced by using an electrostrictive actuator (Queensgate Instruments) attached to a corner cube in the fixed delay line of the probe; the pump−probe optical phase relationship was sinusoidally varied at approximately 100 Hz. Aside from these interference patterns, the measurements revealed no lifetime or decay time beyond the pulse correlation time.

The SHG signal measured in the ATR configuration (Figure 2B) was found to be strongly dependent on the incident angle and was maximal at the ATR minimum (*i.e.*, the SPP resonance). This implies that, as expected,[22] surface SHG is strongly mediated by SPP excitation. Hence, angularly dependent SHG enhancement is a positive indicator of SPP generation. The SH signal detected near time zero was located along the bisector of the two SH rays generated individually by the incident pump and probe beams. This signal along the bisector is due to the interaction of both the pump and probe fields with the material's second-order polarization and is identical to the pump−probe intensity cross-correlation.[26] The temporal profile of this signal is the same as the pulse duration measured from the pump−probe cross-correlation in the BBO doubling crystal (not shown). In fact, this 2ω correlation signal from the film is routinely used to measure and optimize the pulse duration at the interface and serves as a measure of the instrument response function.

Spatial localization of the surface-sensitive optical responses was achieved in the following manner. The optical chopper previously used as a reference for the lock-in amplifier was removed from the experiment and instead the lock-in was referenced to high-frequency (∼2 kHz), small-amplitude (1−10 nm) modulations of the SPM tip−surface separation. Thus, the demodulated signals reveal only the spatially localized optical response due to tip−field coupling within or near the tunneling gap. The time dependent pump−probe and SHG signals have been recorded at single points on the Ag surface as a function of the SPM tip modulation. The waveforms for these measurements are shown in Figure 2C and D; the SPM-modulated fundamental and SHG optical responses are essentially the same as in Figure 2A and B, respectively. These responses were obtained with the probe tip located within the distance for electron tunneling to the surface. Similar signals were observed at several locations on the surface.

B. Surface Plasmon Polariton-Assisted Multiphoton Ionization (SPP-MPI). The SPP-MPI signal is only found when the optical incidence angle is accurately tuned to the ATR resonance for SPP excitation. The detected signal in this case is a photoinduced current. The first important and distinct characteristic of this signal is exhibited in the time domain data shown in Figure 3A, which reveals a large peak at time zero, as well as a superimposed electric-field interference effect (not shown).[27] This SPP-MPI signal is, in fact, a cross-correlation measurement. The temporal dependence shows an instantaneous response which is identical in shape, timing, and width, within the noise limit of the data, to the surface SHG cross-correlation measured simultaneously in the forward direction (Figure 2A).

A second characteristic trait of the SPP-MPI signal is the asymmetric bias dependence, shown in Figure 4A, which increases in magnitude as the bias is changed from 1 V to −10 V.[28] It can be seen that while the signal level increases with increasing negative bias, it does not rise continuously and appears to plateau. These data, as well as the data in Figures 5A and 6A, were acquired at the pump−probe zero-of-time in order to maximize the signal intensity. Additionally, the tip−surface gap for this measurement was set to approximately 50 μm.

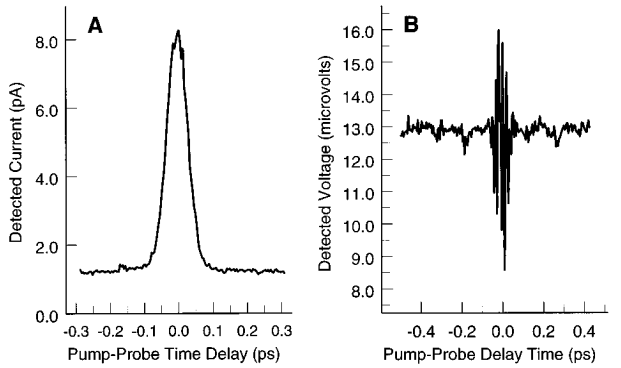

Figure 3. Pump−probe delay time dependence of (A) SPP-MPI, measured at the ATR minimum angle with −5 V bias and ∼50 μm gap, and (B) EFR mechanism, measured away from the ATR minimum angle, with 0 V bias and <10 nm gap.

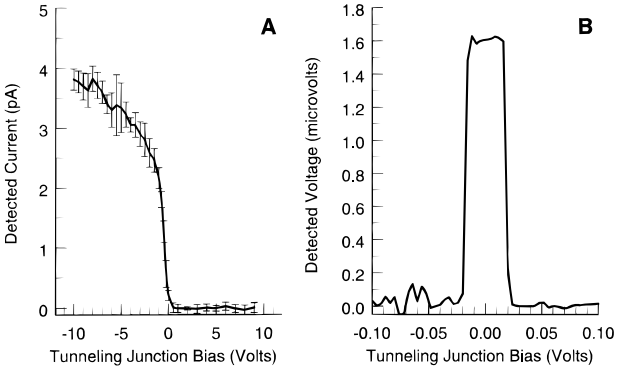

Figure 4. SPM tip−surface junction bias dependence of (A) SPP-MPI, measured at the ATR minimum angle at time zero and with ∼50 μm gap (error bars indicate the standard deviation from over 100 measurements per data point), and (b) EFR mechanism, measured away from the ATR minimum angle with a pump−probe delay time of 1 ps and <10 nm gap.

The third defining characteristic of the SPP-MPI signal is that there is no measurable dependence of the signal on tip distance from the surface over a range from the tunneling regime (0.1−10 nm) up to 4 μm from the surface (the maximum range available from the SPM's piezo). However, as seen in Figure 5A, the signal decays over a range of up to 1000 μm. The maximum signal level is in the range of a few picoamps and decreases nonlinearly by more than an order of magnitude to the noise level over the 1000 μm range. These data are recorded at the pump−probe zero-of-time with −5 V applied bias.

The power dependence of the SPP-assisted signal shown in log−log format in Figure 6A, measured over more than a 10-fold range, exhibits a nonlinear dependence on pump intensity. At lower pump powers, the signal can be approximated as having a second-order dependence while at higher powers the dependence is approximately third order. These data are recorded at the pump−probe zero-of-time with −5 V applied bias.

C. Evanescent Field Rectification (EFR). The second photoinduced mechanism, EFR, is dominant only when the optical incidence angle is detuned from the ATR angle such that SPP generation is no longer resonant. Thus, the dominant process can be expected to result from a mechanism that is not based on SPP or the field enhancement resulting from their excitation.[22] The detected signal in this case is a photoinduced voltage.

The time dependence of the EFR is shown in Figure 3B. Aside from the signal away from the zero-of-time, which is apparently a time independent process and yields a signal on the order of tens or microvolts, the most noteworthy feature of this waveform is the electric field interference pattern centered at time zero. These data were recorded with 0 V applied bias and with a tip−surface gap of approximately 10 nm.

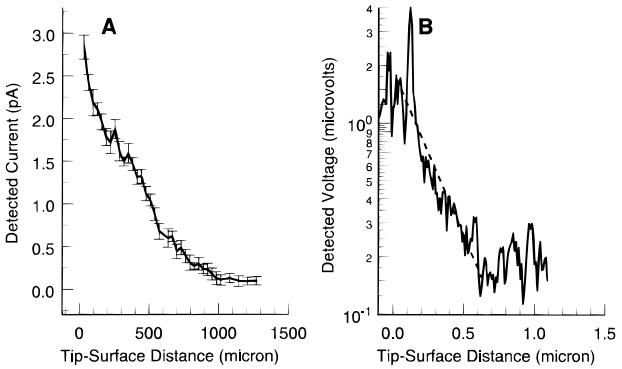

Figure 5. SPM tip−surface gap distance dependence of (A) SPP-MPI, measured at the ATR minimum angle at time zero and with −5 V bias (error bars indicate the standard deviation from over 100 measurements per data point), and (B) EFR mechanism in semilog format (solid line) measured away from the ATR minimum angle with a pump−probe delay time of 1 ps and 0 V bias, with exponential fit (dashed line).

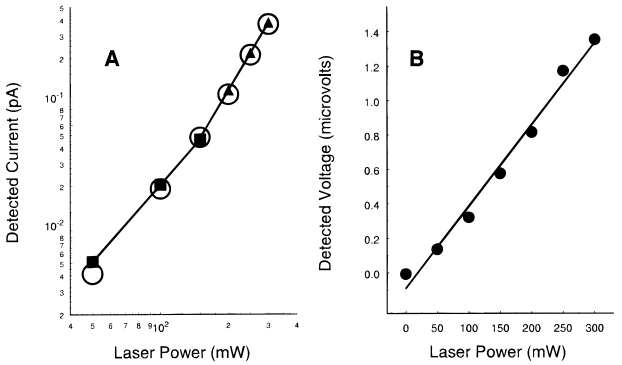

Figure 6. Laser power dependence of (A) SPP-MPI, measured at the ATR minimum angle at time zero with −5 V bias and ∼50 μm gap (circles), along with X^2 (squares and line) and X^3 fits (trianges and line). (B) EFR mechanism, measured away from the ATR minimum angle with a pump−probe delay time of 1 ps, 0 V bias, and <10 nm gap (points) and linear fit.

One of the distinct features of EFR is its dependence on an applied junction bias, shown in Figure 4B. The bias dependence is always observed to have a square-shaped peak centered at 0 V applied bias. The width of the feature shown in Figure 4B is approximately 40 mV (*i.e.*, ±20 mV). This is a typical result and is qualitatively consistent with measurements performed under different conditions; the width of this feature depends on the film thickness and surface quality as well as the tip shape. The bias dependence indicates that an EFR signal is detected only when the amplitude of the static field (due to the applied DC tunneling junction bias) is less than (approximately) 20 mV. These data, as well as the data in Figures 5B and 6B, were recorded with a pump−probe delay time of 1 ps, in order to avoid the complicating interference effect present at time zero. Additionally, the data were recorded with 300 mW laser output power (∼100 mW at the sample) and a tip−surface gap of approximately 10 nm.

The EFR signal has an exponential dependence on the tip distance from the surface. The decay of this signal occurs over the range of approximately 600 nm, as shown in semilog format in Figure 5B, with a decay constant of $(300\ \text{nm})^{-1}$. The exponential decay obtained with the tip approaching the surface is well illustrated in this figure; however, the point of tip−surface contact is not as clearly defined because of the pzt scan method used to approach the surface. The significance of this

signal and the point of tip−surface contact will be discussed below. These data were recorded with a pump−probe delay time of 1 ps and with 0 V applied bias.

Finally, the laser power dependence of the EFR shown in Figure 6B is linear with a fitted slope of 5 μV/W. These data were recorded at the pump−probe delay time of 1 ps and with 0 V applied bias.

IV. Discussion

The nonlocalized temporal responses and SPM-localized pump−probe responses in Figure 2 along with the angle dependent pump−probe data and the bias dependent, distance dependent, and power dependent data presented in Figures 3−6 clearly indicate a sensitivity to surface-mediated photoelectronic processes and that two different photoinduced mechanisms are detected. The differences in the two signals, SPP-MPI and EFR, depend primarily upon the excitation of SPP modes when tuned to the ATR angle or being detuned from this SPP resonance, respectively.

A. Surface Sensitive Optical Spectroscopy. The measurements reflected in Figure 2 were extremely sensitive to the incident angle (<0.1°) of the optical beam to the prism hypotenuse, indicating that the signal involved SPP generation. The forward reflected beams showed, under the proper conditions, a dark horizontal band through the middle of their profile; an effect resulting from the sharp angular dependence of the plasmon absorption resonance.[29] Since only a small portion of the focused beams has the correct momentum matching properties to couple into the SPP, only this portion is significantly absorbed and, hence, attenuated. The angular dependence and the steep slope of attenuation on both sides of the minimum is being exploited in measurements currently in progress to further characterize the relaxation dynamics of hot electrons in thin films.[30]

The pump−probe response from the thin Ag film obtained without the SPM, shown in Figure 2A, exhibits the characteristic pattern of an electric field interference around time zero. The interference results from the pump field being coupled into the probe direction and a heterodyne effect at the detector. The magnitude of the interference was found to be maximal when the incident angle was properly tuned to the ATR minimum, suggesting that the scattering is mediated by SPP generation. Directional light scattering due to SPP excitation is a known phenomenon in ATR devices.[22,31] These interference patterns are the only time dependent features in the pump−probe signal; there is no measurable lifetime or decay time other than the pulse correlation time.[30]

It is, however, expected that the SPP decay or thermalization of hot electrons excited by SPP generation should be evident as a perturbation of the film's dielectric constant and should be observable as a very small transient increase in the reflected probe's intensity.[29] The most probable reason for the lack of an observed relaxation time in these signals is that, as noted above, only a small portion of the beams are on resonance with the SPP and, since the entire reflected probe beam is detected, the relatively small AC signal was not detectable above the noise level of the larger nonresonant probe DC background.[32] A pump−probe response has been observed when detecting only a small solid angle of the probe beam that suggests a plasmon momentum lifetime of about 200 fs.[30]

Results shown in Figure 2C and D have demonstrated the ability to spatially localize surface optical spectroscopy via coupling of the SPM tip to an optical field. Time dependent pump−probe and SHG signals have been recorded at single points on the Ag surface synchronous with SPM tip modulation. The resulting waveforms qualitatively mimic the large-area-averaged surface responses shown in Figure 2A and B. The signals in Figure 2C and D, however, are spatially localized due to coupling of the plasmon to the SPM tip. In these measurements, the tip acts as a localized scattering center to perturb the plane wave SPP. A metal tip is ideal for this measurement, since its inherently large dielectric constant can yield a strong perturbation of the local electronic environment. An optical map of the surface could be produced as a function of the tip position on the surface; such an image with 3 nm lateral resolution has been shown previously by Specht *et al.*[8] However, the current FOS-SPM configuration is designed for femtosecond time resolution in these signals via scanning pump−probe temporal delay. Time-resolved surface "snapshots", including characterization of the method's spatial resolution, will be reported elsewhere.[33]

B. Surface Plasmon Polariton-Assisted Multiphoton Ionization. Photoemission is a well understood phenomenon, with many spectroscopic applications in the study of surfaces and interfaces. For example, ionization processes in metal films have been previously demonstrated and studied in the Kretschmann−Raether ATR geometry.[34,35] Multiphoton ionization was shown to be an effective means of obtaining cross-correlation measurements of different color optical pulses where no convenient nonlinear mixing crystal was available.[34] Tsang *et al.*[35] have examined the SPP-MPI process on several metal films, including silver, showing pump−probe temporal signals peaked at the zero-of-time with no other temporal dependence. In the case of silver the SPP-MPI signal had the same shape as the SH cross-correlation, indicating, along with its power dependence, that the SPP-MPI signal results from a process of the same order as the SH correlation (*i.e.*, second order). The energy of the 620 nm (*i.e.*, 2 eV) pulses employed in ref 35 is consistent with the reported work function (Φ = 3.5 eV, for a thin silver film) being accessible via a two-photon process.

In the present work, the temporal data of Figure 3A show an absence of broadening of the time domain signal with respect to the SH cross-correlation (Figure 2B), indicating that the pump pulse does not prepare a population in a state between the Fermi level and the vacuum level, such as an image-potential state.[36,37] Since there is no lifetime (broadening) exhibited in the response, the pump−probe response is the pulse cross-correlation. In other words, on the basis of the equivalence of the time domain signal and the SH cross-correlation, it can be concluded that population of an intermediate state below the vacuum level by a single photon process, such as resonance-enhanced multiphoton ionization, is ruled out for the SPP-assisted time domain response presented here. Further, from the absence of any broadening of this response, as compared to the pulse correlation, it is reasonable to conclude that the electron emission is, in fact, due to the quantum MPI process and not thermal emission. This is clear, since thermionic emission is know to yield thermal lifetimes greater than 1 ps.[38] This direct excitation of electrons, without lattice heating, is consistent with a number of studies which have found that a femtosecond excitation pulse prepares nonequilibrium electron and lattice temperatures in metals.[39−42] This situation can be attributed to an electron−phonon energy transfer time that is long compared to the pulse duration. Consequently, the absorption depth (*i.e.*, $1/a$, where a is the absorption coefficient) is greater than the thermal diffusion length ($l_{th} = [Dt]^{1/2}$, where D is the thermal diffusivity and t is the pulse width). In the present case, with 40 fs pulses near 800 nm, the absorption depth is approximately 12 nm in

silver while the thermal diffusion length is approximately 2.5 nm.[41] One result of the greater absorption depth is that pure electronic excitations can be created and probed, without the effect of thermalization and lattice heating.

The most unique characteristic of the SPP-MPI signal is that there is no measurable dependence of the signal on tip distance from the surface over the range from the tunneling regime to 4 μm from the surface; the lack of decay over this range is inconsistent with a signal based on a tunneling-mediated mechanism. Instead, Figure 5A shows that the signal decays over a range of up to 1000 μm. This distance dependence is not consistent with a mechanism based on the direct interaction of the SPM tip with either a SPP or an evanescent field, which decays over $\sim$0.5 μm on an Ag film for optical wavelengths.[8,22] However, for the case of the SPP-MPI mechanism, the long-range distance dependence is the expected result.

The only predicted effect of having the metal tip close to the surface ($<$0.5 μm) would be its effect as a localized perturbation due to coupling with the optical field or scattering of SPP's,[8,11] as was seen in the surface sensitive optical spectroscopy results discussed previously. While a tip-induced perturbation of SPP generation should, in principle, exist, no clear evidence of this effect has been seen for a number of reasons. The tip employed in these measurements was not insulated around its sides and hence could pick up signals resulting from a larger region than just the area immediately below its apex. Thus, a perturbation of the SPP's induced in this area by the close proximity of the tip to the surface would only be a small contribution to the total ionization signal and may be below the noise level of the distance dependent data. However, this effect (*i.e.*, a localized perturbation due to tip−sample interactions) may account for the initially steep slope of the data in Figure 5A. This point is under further investigation. In continuing work, the same studies are being performed with insulated STM tips that leave only the apex clean to detect the MPI signal. In principle, this will enhance local sensitivity as is the case for electrochemical STM.[43] Insulated tips may facilitate detection of tip-induced perturbations of SPP generation and the consequential effect on the MPI process; perturbations of this type might be exploited for enhanced contrast and imaging in FOS-SPM measurements.

The long-range distance dependence is fully consistent with the detection of ionized electrons, which have no difficulty traveling millimeter distances when given a bias to drive them.[35,44] This millimeter-range distance dependence is an important measurement for the characterization of the SPP-MPI mechanism and for distinguishing it from the EFR process. Clearly, the range of 10^{-3} to 10^{-7} m is not appropriate for nanometer scale spatial resolution. Rather, scanning of mesoscopic features must be carried out close to the surface, likely in the range 0.1−10 nm. As noted above, this would include the use of an insulated tip to limit the detected signal to a localized area and may also exploit localized interactions of the tip with SPP generation.

The asymmetric bias dependence of the SPP-MPI signal in Figure 4A increases with bias changes from 1 V to −10 V. As noted previously, this bias dependence is consistent with electrons generated at the surface being drawn more efficiently to the anode (*i.e.*, the tip) as the bias is increased in the appropriate direction. While the signal level rises with increasing negative bias, there is a "saturation" effect at the largest biases, approaching its maximal value at a large negative bias. This suggests that the collection efficiency is less than 100% at low bias. This conclusion would not be surprising, since even the collection fields used here (0−20 V/mm, at a 500 μm gap) are, in fact, small as compared to the kilovolt per millimeter fields commonly used for efficient electron collection.[35]

Thermal Effects. Thermal effects must be considered in the interpretation of the current results; the most significant effect, given the proximity of the tip and sample, is thermal expansion. Thermal expansion has been found to result primarily from the heating of an STM tip due to coupling with SPP's at the sample interface. The consequence of this expansion is a reduction of the tunneling gap and an exponential increase in the tunneling signal. This effect was exploited by Rücker *et al.* to yield enhanced contrast in STM imaging.[9] In the present case, the results argue against the presence of a significant thermally induced signal due to effects such as tip heating and expansion. First, this effect could only be significant when the tip is close to the surface (*i.e.*, within the tunneling regime) where even small-scale thermal expansion is large and relevant in proportion to the 10 Å gaps being measured. However, the distance dependent results in Figure 5A show that the photoinduced signal is present at both small and large gap spacings. Second, the bias dependence for such a process on a metal would be expected to be symmetric in magnitude about 0 V and increase with increasing voltage.[45] Expansion would cause the gap spacing to decrease and result in an increased signal equivalently for applied voltages in either direction. However, the asymmetric bias dependence shown in Figure 4A clearly conflicts with a photoinduced signal based on thermal expansion. Third, the magnitude of such expansion scales with the amount of heat absorbed per modulation cycle,[9] hence inversely proportional to the chopper frequency. However, the signals were observed to be independent of chopper frequency.

It is clear that there is, however, some heating and hence expansion, at least in the sample, due to absorption of the incident light. Given that there is approximately 10% absorption of the 0.5 nJ incident pulse by the Ag film, the temperature rise per pulse is on the order of 0.1 °C.[46] The resultant amount of thermal expansion per pulse is very small, on the basis of a thermal expansion coefficient which is on the order of 10^{-5} $°C^{-1}$.[47] During the 0.5 ms when the optical chopper is open and given the 90 MHz repetition rate of the laser, there is a reasonably large amount of energy absorbed into the film. However, it is difficult to estimate the magnitude of any temperature change during the chopper half-cycle without accurately knowing the volume that is heated, which is uncertain due to thermal diffusion throughout the film and into the relatively massive fused silica substrate, which can function as a heat sink. Thus, it is not possible to calculate thermal expansion of the sample or thermoelectric emf's[13] which may arise from differential heating across the gap. Nevertheless, any effect of differential heating or thermal expansion of the tip or sample would appear only as a DC offset in the lock-in demodulated time domain data and not contribute to the transient wave form on femtosecond to picosecond delay times. The high repetition rate laser system has a pulse-to-pulse period that is comparable to the thermal diffusion time of silver.[32] Thus, between successive pump−probe pulse pairs, the system lacks the time to cool significantly and is consequently near a thermal steady state during the measurement. Thus, while thermal effects are to be expected and have to be carefully accounted for in the case of imaging with a small tip−surface separation, there do not appear to be any thermal contributions to the signals presented herein.

It is clear from the results shown in Figure 4A that the SPP-MPI bias dependent data has no contribution from the evanescent field rectification mechanism at 0 V applied bias. The lack of a contribution from the EFR mechanism to the SPP-

MPI signal can be understood on the basis of the tip−surface gap conditions under which the SPP-MPI data was recorded. This gap distance, approximately 50 μm, is simply beyond the range of the evanescent field mechanism. Therefore, although the two mechanisms may coexist near the surface with a small applied bias, at ranges on the order of 10's of microns and/or a large negative bias, only the SPP-MPI mechanism contributes to the detected signal. Under scanning conditions, where the tip would be close to the surface, it would be necessary to use the applied bias thoughtfully to isolate one photoinduced mechanism at a time.

Power Dependence. The SPP-MPI signal dependence on laser power, which reveals the interaction order of the signal mechanism, has significance for the characterization of the signal as a MPI mechanism. For a multiphoton mechanism, the signal scales as I^n, where I is the intensity and n is the order of interaction. In the present data, as shown in Figure 6A, the interaction order was determined to be approximately 2, for lower optical power, and 3 for higher power. Thus, the signal results from both second-order and third-order, or two- and three-photon, processes.

From the power dependence of this signal, *i.e*., the implied two-photon process at lower power, and since ionization requires multiphoton energy greater than or equal to the work function, Φ, then $\Phi \leq 3.2$ eV (2×1.6 eV). This value is 25% lower than the work function of bulk silver ($\sim$4.3 eV)[47] and 10% lower than the value reported by Tsang *et al*. for a thin Ag film (3.65 eV).[35] However, it has been shown under UHV conditions that dosing Ag films with water can lower the work function by as much as 0.6 eV.[48] Since the present experiments were performed in air, there is certainly a water adlayer surface contamination that is always present. Another study of SPP-MPI from Ag films reports a one-photon dependence for 3.49 eV photons, a two-photon dependence for 2.33 eV photons, and a three-photon dependence for 1.16 eV photons.[49] From this it can be deduced that the work function for thin Ag films is in the range 2.3−3.5 eV. We, therefore, suggest that the *work function of our 525 Å Ag film at some sites on the surface is less than or equal to 3.2 eV* and that ionization can result from a two-photon process. However, the apparent three-photon MPI process measured at high powers implies that other sites on the surface, or the remainder of the surface sites, have a work function in the range 3.2−4.8 eV. Identification of localized surface sites with different reactivity is an important aspect of the continuing work on this project.

C. Evanescent Field Rectification. The second photoinduced mechanism, EFR, is due to a nonlinear optical process occurring at the interface. Optical rectification is a well understood phenomenon and, as noted by Shen, one of the first nonlinear optical effects to have been discovered.[50−52] The nonlinear polarization due to optical rectification is given as

$$P^{(2)}(0) = \chi^{(2)}(0 = \omega - \omega):E(\omega)E^*(\omega)$$

where $\chi^{(2)}$, the nonlinear susceptibility, along with the applied fields at frequency ω, governs the magnitude of the effect. The induced voltage due to this effect is proportional to the nonlinear polarization. Hence, a measure of this induced voltage is a measure of the nonlinear phenomenon, *i.e*., optical rectification.

Experimentally, the EFR signal is reproducibly measured in the SPM tip−surface gap by tilting the prism slightly off the ATR minimum angle. Thus, the measured signal is either due to a process initiated by the evanescent optical field decaying exponentially from the silver film's surface or is due to a weak SPP field. Since SPP generation is extremely sensitive to incident angle and is maximal near the ATR minimum, SPP excitation away from the ATR angle can only result from the coupling to or scattering by localized roughness or other surface features.[48,53] However, for the case of a smooth film, this SPP excitation process is relatively weak as compared to the angularly tuned momentum matched excitation at the ATR resonance angle. The EFR signal has an exponential dependence on the tip distance from the surface with a decay constant of $(300\ \text{nm})^{-1}$. The exponential decay is illustrated in Figure 5B, even though the point of tip−surface contact is not as clearly defined.[54−56] The observed exponential decay of the signal compares well with the decay range of the evanescent optical field, which couples through the film, as well as the decay range of Ag's SPP at this wavelength.[8,22,57] However, since the film orientation is adjusted to be away from the ATR minimum (where SPP generation is a maximum) and the narrow bias dependence of this signal is symmetric about zero, it follows that this signal is dominated by EFR and not a MPI mechanism.

The most noteworthy feature of the temporal waveform shown in Figure 3B is the interference pattern at time zero. The amplitude of the interference is approximately symmetric above and below the baseline, suggesting that the pattern is an electric-field interference resulting from the simultaneous arrival of both the pump and the probe pulses in the tunneling gap. This is consistent with the expect response of a $\chi^{(2)}$ process, although this response may exist in the case of higher order nonlinear processes as well. However, the laser power dependence of the EFR is found to be highly linear with a fitted slope of 5 μV/W. Theoretically, a $\chi^{(2)}$ process, such as optical rectification, has a second-order dependence on the oscillating field amplitude; this would correspond to a linear dependence on laser power and is consistent with the present results.

One of the distinct features of the EFR signal is its dependence on the junction bias shown in Figure 4B, which is a square-shaped peak of $\pm$20 mV width centered at 0 V. The symmetric bias dependence of the evanescent field EFR signal is consistent with a mechanism based on optical rectification. Cutler *et al*.[58] showed that optical rectification in a tunneling gap will occur while the static DC field (generated by the applied bias across the gap) is smaller in magnitude than the oscillating optical field. The calculated amplitude of the DC field in the tunneling gap at 20 mV is on the order of 10^6 V/m for a gap spacing of ten nanometers. A field strength of 10^6 V/m is almost exactly the field amplitude for 40 fs pulses with 3 nJ pulse energy (10^5 W peak power) focused to a 50 μm radius beam waist.[59] On the basis of this calculation it is concluded that the signal is likely due to rectification of the evanescent field.

The signal obtained for voltages below -25 mV is noisier than the signal above $+25$ mV. This asymmetry, which cannot be attributed to an evanescent field rectification, may be due to a weak SPP-MPI process, since SPP-MPI signals are enhanced at negative voltages (see preceding subsection). Thus, both EFR and SPP-MPI may be coexisting mechanisms; however, it is clear that under the given conditions the rectification mechanism dominates near zero bias.

Previous measurements and calculations of the rectified current as a function of STM tip−sample distance reveal a decay of the signal over a range of 10's of angstroms.[58] There are, however, several significant differences between that work and the present situation, so direct comparison cannot be made. For example, the calculations of ref 58 involve a gold surface and a tungsten tip, which have work functions different from the thin Ag film and the Pt:Ir tip used in the present experiment. Nevertheless, both qualitative and semiquantitive agreement

exists, particularly, the exponential dependence of EFR on gap distance as well as the symmetric bias dependence.

Some of the present results are, however, not qualitatively consistent with those expected for optical rectification in the tunneling regime.[58] For example, on the basis of theory one would expect the width of the bias resonance to narrow with the square root of the laser power, yet no narrowing was observed. Furthermore, the rectification mechanism discussed by Cutler *et al*.[58] and Hagmann[60] results from the response of the tunneling electrons to the oscillating optical fields. Thus, beyond the tunneling regime (∼0.1−10 nm) it is clear that one would not expect a rectification signal involving tunneling electrons. Since the rectification signal measured here decays exponentially over 100's of nanometers, it cannot be attributed to perturbed tunneling electrons. While the data recorded beyond the tunneling gap can be clearly identified as EFR due to the nonlinear polarization driven by the evanescent field, it is not yet clear why the bias dependence, which is qualitatively consistent with an optical field rectification mechanism in the tunneling gap, shows the symmetric dependence. Continuing work on understanding the bias dependence includes an analysis of the width as a function of film thickness, film composition, optical band widths, and collimation conditions.

V. Conclusion

In conclusion, FOS-SPM has been shown to be a viable technique for correlated spatial and temporal resolution of optically initiated dynamics at an interface. The results given here demonstrate that femtosecond time resolution of spatially localized optical measurements is obtained through optical field coupling to SPM tip motion. Pump−probe and SHG results have been presented to illustrate this effect. Time-resolved SPM measurements of optoelectronic processes were shown. This time resolution, on the scale of femtoseconds, is provided by an optical pump−probe correlation method. Finally, it has been shown that FOS-SPM can identify and differentiate between different optically induced optoelectronic processes.

Two distinct mechanisms for photoinduced signal generation have been established for the Ag surface air−metal interface under investigation. The first of these is a surface plasmon polariton-assisted multiphoton ionization process. The second is evanescent field optical rectification at the interface. These two mechanisms have been identified and distinguished from each other by measuring and analyzing their dependence on several variables, including optical incidence angle, tunneling junction bias, optical pump−probe time delay, laser power, as well as the SPM tip-to-surface distance.

Scanning optical microscopies (SOM) (*i.e*., near-field scanning optical microscopy (NSOM), photon scanning tunneling microscopy (PSTM), *etc*.) are other techniques that allow for simultaneous spatial and temporal resolution.[61−63] One difference between these techniques and FOS-SPM is that the spatial resolution in SOM is many 10's of nanometers as compared with the subangstrom level that STM achieves at its best. However, the most important advantage of FOS-SPM over scanning optical microscopies is the potential not only to extract spectroscopic information but also to measure directly the electronic local density of states of the system under investigation.

The FOS-SPM technique and equipment are being further improved to allow for reliable four-dimensional space and time dependent measurements of surfaces. Signal averaging is required to produce these signal, and thus, in order to produce a full 3-D map of the surface as a function of pump−probe delay time, reproducible absolute positioning of the SPM tip is required without drift, creep, or hysteresis. Consequently, continued technical work on this project includes upgrading the SPM scanner to allow for absolute positioning via a capacitance feedback mechanism. Following this modification it will also be possible to characterize the extent of localization and the spatial resolution of the FOS-SPM technique.

As noted previously, scanning of mesoscopic features will necessarily be carried out with the SPM tip close (0.1−10 nm) to the surface. For SPP-MPI measurements, the tip will need to be insulated, as is done in STM studies in electrochemical cells, to limit the detection of spurious signals arising from other than below the apex in the tunneling gap.[43] Additionally, careful adjustment, and perhaps modulation, of the applied bias will be required to determine and control the dominant optoelectronic mechanism being detected. Further attention will also need to be focused on the influence of thermal effects when the tip−surface gap is within the tunneling regime. Continued progress in these technical areas will lead toward the ability to map out spatially-localized photoinduced excitations of surfaces and surface adsorbates as a function of time on the femtosecond scale and hence *the potential for correlating surface features with reactivity* (*e.g*. sources of below bulk work function electrons).

Studies based on the FOS-SPM technique will have broad potential application, including studies of surface-mediated catalysis and, as suggested by Douketis *et al*.,[48] roughness-enhanced multiphoton ionization. These studies may be useful in analyzing and understanding how surface structure may be correlated with photoelectronic reactivity. For example, the two- and three-photon dependences for the SPP-MPI mechanism presented in this work suggest that different sites on the surface have different work functions. An experimental understanding of this phenomenon would benefit the understanding of surface photochemistry in general and specifically may be applicable to the design of optoelectronic devices. Furthermore, application of FOS-SPM to the study of thin films, such as conducting polymers, chemi- and physisorbed particles, nanocrystals, and other nanotechnology, should provide important understanding of localized photoexcitation and reaction dynamics. The ability to measure directly temporal dynamics of photoexcited carriers would be an important tool for the development and characterization of nanoscale optoelectronic switches.[64]

Note Added in Proof. Correlated and simultaneous STM topography and SPP-MPI images have recently been obtained using a custom designed position stabilized STM. Constant height measurements with insulated tips within the STM-tunneling regime suggest that the ionization is nonuniform over the surface and appears to correlate with surface roughness features. These results will be presented elsewhere.[33]

Acknowledgment. The authors would like to thank B. Romanow of the LRSM for providing the thin films used in this study. We acknowledge financial support from the Deutsche Forschungsgemeinschaft, University of Pennsylvania MRL (Grant DMR-91-20668), and National Science Foundation SGER Grant CHE-9311337. N.F.S. is the recipient of a David and Lucille Packard Foundation fellowship and is an Arnold and Mabel Beckman Foundation Young Investigator.

References and Notes

(1) Cavanagh, R. F.; King, D. S.; Stephenson, J. C.; Heinz, T. F. *J. Phys. Chem*. **1993**, *97* (4), 786−798.

(2) Lanzafame, J. M.; Palese, S.; Wang, D.; Miller, R. J. D.; Muenter, A. A. *J. Phys. Chem*. **1994**, *98* (43), 1020−11033.

(3) Wiesendanger, R. *Scanning Probe Microscopy and Spectroscopy*; Cambridge University Press: Cambridge, 1994.

(4) Hamers, R. J. *Annu. Rev. Phys. Chem.* **1989**, *40*, 531.
(5) Fleming, G. *Chemical Applications of Ultrafast Spectroscopy*; Oxford University Press: New York, 1986.
(6) Polanyi, J. C.; Zewail, A. H. *Acc. Chem. Res.* **1995**, *28* (3), 119−132.
(7) Becker, P. C.; Fragnito, H. L.; Bigot, J. Y.; Brito Cruz, C. H.; Shank, C. V. *Phys. Rev. Lett.* **1989**, *63* (5), 505−507.
(8) Specht, M.; Pedarnig, J. K.; Heckl, W. M.; Hänsch, T. W. *Phys. Rev. Lett.* **1992**, *68* (4), 476−9.
(9) Rücker, M.; Knoll, W.; Rabe, J. P. *J. Appl. Phys.* **1992**, *72* (11), 5027−31.
(10) Völcker, M.; Krieger, W.; Walther, H. *Phys. Rev. Lett.* **1991**, *66* (13), 1717−20.
(11) Bachelot, R.; Gleyzes, P.; Boccara, A. C. *Opt. Lett.* **1995**, *20* (18), 1924−1926.
(12) Gorbunov, A. A.; Pompe, W. *Phys. Status Solidi A* **1994**, *145*, 333−8.
(13) Kuk, Y.; Becker, R. S.; Silverman, P. J.; Kochanski, G. P. *Phys. Rev. Lett.* **1990**, *65* (4), 456−9.
(14) Akari, S.; Lux-Steiner, M. Ch.; Vögt, M.; Stachel, M.; Dransfeld, K. *J. Vac. Sci. Technol., B* **1991**, *9* (2), 561−3.
(15) Bonnell, D. A.; Rohrer, G. S.; Frank, R. H. *J. Vac. Sci. Technol., B* **1991**, *9* (2), 551−556.
(16) Hamers, R. J.; Cahill, D. G. *J. Vac. Sci. Technol., B* **1991**, *9* (2), 514−8.
(17) Nunes, G., Jr.; Freeman, J. *Science* **1993**, *262*, 1029−32.
(18) Weiss, S.; Ogleres, D. F.; Botkin, D.; Salameron, M.; Chemla, D. S. *Appl. Phys. Lett.* **1993**, *63* (18), 2567−9.
(19) Gerber, G.; Sattler, F.; Vögler, S.; Grand, J. R.; Leiderer, P.; Möller, R. *Ultrafast Phenomena IX*; Barbara, P. F., Knox, W. H., Mourou, B. A., Zewail, A. H., Eds.; Springer-Verlag: Berlin, 1994; pp 149−50.
(20) Tersoff, J.; Hamann, D. R. *Phys. Rev. B* **1985**, *31*, 805.
(21) Bian, R. X.; Dunn, R. C.; Xie, X. S.; Leung, P. T. *Phys. Rev. Lett.* **1995**, *75* (26), 4772−5.
(22) Raether, H. *Surface Plasmons*; Springer-Verlag: Berlin, 1988.
(23) Burstein, E.; Chen, W. P.; Chen, Y. J.; Hartstein, A. *J. Vac. Sci. Technol.* **1974**, *11* (6), 1004−1019.
(24) Asaki, M. T.; Huang, C. P.; Garvey, D.; Zhou, J.; Kapteyn, H. C.; Murnane, M. M. *Opt. Lett.* **1993**, *18*, 977−979.
(25) The film thickness was determined by monitoring a crystal sensor during deposition. The uncertainty in this thickness is on the order of ±25 Å.
(26) With the exception of scatter, consideration of wave vector matching conditions shows that this signal can only be due to the equal interaction of both fields in the material.
(27) The interference pattern can be washed out by small modulations of the probe path length, as has been done for the signals recorded and presented in Figures 3A−6A.
(28) The tip is at ground relative to surface voltage; therefore, at negative bias the electron flow is from the surface to the tip.
(29) Groeneveld, R. H. M.; Sprik, R.; Lagendijk, A. *Phys. Rev. Lett.* **1990**, *64* (7), 784−7.
(30) Wang, W.; Feldstein, M. J.; Scherer, N. F. *Chem. Phys. Lett.*, submitted.
(31) Simon, H. J.; Guha, J. K. *Opt. Commun.* **1976**, *18* (3), 391−394.
(32) van Exter, M.; Lagendijk, A. *Phys. Rev. Lett.* **1988**, *60* (1), 49−52.
(33) Feldstein, M. J.; Scherer, N. F. Work in progress.
(34) Muggli, P.; Brogle, R.; Joshi, C. J. Opt. Soc. Am. B **1995**, *12* (4), 553−8.
(35) Tsang, T.; Srinivasan-Rao, T.; Fischer, J. *Phys. Rev. B* **1991**, *43* (11), 8870−8.
(36) Schoenlein, R. W.; Fujimoto, J. G.; Eesley, G. L.; Capehart, T. W. Phys. Rev. Lett. **1988**, *61* (22), 2596−99.
(37) Lingle, R. L.; Padowitz, D. F.; Jordan, R. E.; McNeill, J. D.; Harris, C. B. *Phys. Rev. Lett.* **1994**, *72* (14), 2243−2246.
(38) Riffe, D. M.; Wang, X. Y.; Downer, M. C.; Fisher, D. L.; Tajima, T.; Erskine, J. L.; More, R. M. *J. Opt. Soc. Am. B* **1993**, *10* (8), 1424−1435.
(39) Fujimototo, J. G.; Liu, J. M.; Ippen, E. P.; Bloembergen, N. *Phys. Rev. Lett.* **1984**, *53* (19), 1837−1840.
(40) Preuss, S.; Demchuk, A.; Stuke, M. *Appl. Phys. A* **1995**, *61*, 33−37.
(41) Pronko, P. P.; Dutta, S. K.; Squier, J.; Rudd, J. V.; Du, D.; Mourou, G. *Opt. Commun.* **1995**, *114*, 106−110.
(42) Aeschlimann, M.; Schmuttenmaer, C. A.; Elsayed-Ali, H. E.; Miller, R. J. D.; Cao, J.; Gao, Y.; Mantell, D. A. *J. Chem. Phys.* **1995**, *102* (21), 8606−8613.
(43) Fan, F. R. F.; Bard, A. J. *Science* **1995**, *267* (5), 871−874.
(44) Kadyshevitch, A.; Naaman, R. *Phys. Rev. Lett.* **1995**, *74* (17), 3443−3446.
(45) Möller, R.; Albrecht, U.; Boneberg, J.; Koslowski, B.; Leiderer, P.; Dransfeld, K. *J. Vac. Sci. Technol., B* **1991**, *9* (2), 506−509.
(46) The temperature rise is calculated by assuming that the heated volume is a cylinder with a radius equal to the beam size (50 μm) with a height equal to the absorption depth (12 nm) with the specific gravity (10.5) and the specific heat (0.252 J g^{-1} $°C^{-1}$) of Ag.[46]
(47) Lide, D. R., Ed. *CRC Handbook of Chemistry and Physics*, 74th ed.; CRC Press: Boca Raton, FL, 1993.
(48) Douketis, C.; Shalaev, S. M.; Haslett, T. L.; Wang, Z. H.; Moskovits, M. *J. Electron Spectrosc. Relat. Phenom.* **1994**, *64* (5), 167−175.
(49) Chen, H.; Boneberg, J.; Leiderer, P. *Phys. Rev. B* **1993**, *47* (15), 9956−8.
(50) Shen, Y. R. *Principles of Nonlinear Optics*; J. Wiley: New York, 1984; pp 57−59.
(51) Bass, M.; Franken, P. A.; Ward, J. F.; Weinreich, G. *Phys. Rev. Lett.* **1962**, *9* (11), 446−448.
(52) Ward, J. F. *Phys. Rev.* **1966**, *143* (2), 569−574.
(53) Ritchie, G.; Burstein, E.; Stephens, R. B. *J. Opt. Soc. Am. B* **1985**, *2* (4), 544−551.
(54) The contact point has been estimated in the current data, and the zero point on the distance axis has been defined on the basis of this estimate. Once the tip has established full contact with the film, the signal level is flat as a function of voltage applied to the SPM *Z*-axis piezo. Between this flat region and the exponential decay there are a number of spikes in the signal that we believe can be attributed to (1) an additional signal from being with in the tunneling regime (less than 10's of nanometers from the surface)[55] and (2) noise associated with crashing the tip into the thin metal film.[56]
(55) Jericho, M. H.; Blackford, B. L.; Dahn, D. C. *J. Appl. Phys.* **1989**, *65* (12), 5237−9.
(56) Taylor, P.; Williams, R. S.; Chi, V. L.; Bishop, G.; Fletcher, J.; Robinett, W.; Washburn, S. *Surf. Sci.* **1994**, 306 (1−2), 534−8.
(57) van Hulst, N. F.; Segerink, F. B.; Bölger, B. *Opt. Commun.* **1992**, *87* (5, 6), 212.
(58) Miskovsky, N. M.; Park, S. H.; Culter, P. H.; Sullivan, T. E. *J. Vac. Sci. Technol., B* **1994**, *12* (3), 2148−52. Nguyen, H. Q.; Cutler, P. H.; Feuchtwang, T. E.; Huang, Z.; Kuk, Y.; Silverman, P. J.; Lucas, A. A.; Sullivan, T. E. *IEEE Trans. Electron Devices* **1989**, *36* (11), 2671−8.
(59) To calculate these values, we use the following relations

$$F_{dc} = \frac{V_{dc}}{\text{gap}}; \quad [V_{dc} = 0.020\ \text{V}, \quad \text{gap} = 10 \times 10^{-9}\ \text{m}]$$

$$= 2 \times 10^6 \frac{\text{V}}{\text{m}}$$

$$F_{os} = \left(\frac{2\frac{P}{2\pi r^2}}{c\epsilon_0}\right)^{1/2}; \quad P_{pk} = \frac{P_{av}}{\text{rep rate} \times \text{pulse duration}}$$

$[P_{av} = 0.300\ \text{W}, \text{rep rate} = 100\ \text{MHz},$
$\text{pulse duration} = 40\ \text{fs}, r = 50 \times 10^{-6}\ \text{m}]$

$$= 2 \times 10^6 \frac{\text{V}}{\text{m}}$$

(60) Hagmann, M. J. *Appl. Surf. Sci.* **1995**, 87−88 (1−4), 368−372.
(61) Dunn, R. C.; Allen, E. V.; Joyce, S. A.; Anderson, G. A.; Xie, X. S. *Ultramicroscopy* **1995**, *57*, 113−117. Dunn, R. C.; Xie, X. S. *Ultramicroscopy* **1995**, *57*, 169−172. Xie, X. S.; Dunn, R. C. *Science* **1994**, *265*, 361−364.
(62) Smith, S.; Orr, B. G.; Kopelman, R.; Norris, T. *Ultramicroscopy* **1995**, *57*, 173−175.
(63) Stark, J. B.; Mohideen, U. *Quantum Electronic Conference*; OSA Technical Digest Series 16; Optical Society of America; Washington, D.C., 1995; pp 83−84.
(64) Koshland, D. E., Jr. Ed. Science **1991**, *254*, 1300−1341.

JP9517918